Hybrid Electrophototroph Enables High-Efficiency Carbon Dioxide Valorization to Fuel Molecules

Zhaodong Li
National Renewable Energy Laboratory
Chao Wu
National Renewable Energy Laboratory
Xiang Gao
National Renewable Energy Laboratory
Bennett Addison
National Renewable Energy Laboratory
Xihan Chen
National Renewable Energy Laboratory https://orcid.org/0000-0001-7907-2549
Jianping Yu
National Renewable Energy Laboratory
Drazenka Svedruzic
National Renewable Energy Laboratory
Jeffrey Blackburn
National Renewable Energy Laboratory
Wei Xiong (Wei.Xiong@nrel.gov)
National Renewable Energy Laboratory

Article

Keywords: Artificial Photosynthesis, Photosynthetic Electron Transfer Chain, Cyanobacteria, Bioelectrochemical Hybrid

Posted Date: October 30th, 2020

DOI: https://doi.org/10.21203/rs.3.rs-93987/v1

Hybrid Electrophototroph Enables High-Efficiency Carbon Dioxide Valorization to Fuel Molecules

Zhaodong Li[1], Chao Wu[2]†, Xiang Gao[2]†, Bennett Addison[2], Xihan Chen[1], Jianping Yu[2], Drazenka Svedruzic[2], Jeffrey Blackburn[1]*, Wei Xiong[2]*

[1]Materials Science Center, National Renewable Energy Laboratory, Golden, CO.

[2]Biosciences Center, National Renewable Energy Laboratory, Golden, CO.

* Correspondence to: Jeffrey.Blackburn@nrel.gov and Wei.Xiong@nrel.gov

† Denotes equal contribution

Abstract

Nature's biocatalytic processes are driven by photosynthesis, whereby photosystems I and II are connected in series for light-stimulated generation of fuel products or electricity. Externally supplying electricity directly to the photosynthetic electron transfer chain (PETC) has numerous potential benefits, although strategies for achieving this goal have remained elusive. Here we report an integrated photo-electrochemical architecture which shuttles electrons directly to PETC in living cyanobacteria. The cathode of this architecture electrochemically interfaces with cyanobacterial cells lacking photosystem II activity that cannot perform photosynthesis independently. Illumination of the cathode channels electrons from external circuit to intracellular PETC through photosystem I, ultimately fueling CO_2 conversion to acetate, a model fuel molecule with 9.32% energy efficiency, exceeding the efficiency of natural photosynthesis in higher plants (<1%) and cyanobacteria (~4-7%). The resulting "Electrophototrophic" bio-electrochemical hybrid has the potential to produce fuel chemicals with numerous advantages over standalone natural and artificial photosynthetic approaches.

Main

Electrification of biocatalysis represents a strategic direction to meet global energy demand and foster development of efficient systems for conversion of CO_2 to fuels and chemical feedstocks[1-3]. In nature, photosynthesis drives biocatalytic processes that form the basis of life on Earth by converting light energy to the chemical energy utilized for endergonic metabolism[4]. The central photosynthetic process involves coupled photoexcitation of two reaction center photosystems (PS) I and II (Fig. 1a). Excitation of PSI initiates electron transfer to ferredoxin and NADPH that energizes CO_2-fixing pathways such as the Calvin-Benson-Bassham (CBB) cycle [5]. Photoexcitation of PSII results in oxygen evolution and electron transport from water to plastoquinone (PQ), which then regenerates neutral PSI through a series of reactions in the photosynthetic electron transfer chain (PETC)[5].

Substantial research efforts have focused on leveraging biological photosystems (*e.g.* in algae and cyanobacteria) for sustainable production of energy products from sunlight[6 7]. For example, photosynthetic cyanobacteria have been engineered to produce fuel chemicals and polymers from CO_2[8-13]. However, natural photosynthesis cannot use the full terrestrial solar irradiance, since photosynthetically active radiation (PAR) is limited to a subset of visible light (mostly 400-500 nm and 600-700 nm). Additionally, the natural photosynthetic CO_2 fixation efficiency is diminished by the photorespiration process[14]. Artificial photosynthetic solar-to-fuels cycles have been proposed as alternatives to natural photosynthesis[15-17]. These cycles can achieve high intrinsic energy efficiencies, but typically terminate at hydrogen and struggle to produce carbon-based biofuels at high energy and carbon conversion efficiencies[18]. We hypothesize that the ultimate goal of producing high-order carbon products at high energy efficiency may be achieved by interfacing natural and artificial photosynthesis in a hybrid system where a photosynthetic organism is synergistically energized by exogenous electrons through PETC. In the inverse of this process, photosynthetic fuel cells utilize “photo-electrogenic” microbes to generate electrical currents [19-22]. However, to date there is no integrated electron transfer strategy that generates chemical energy upon external supply of electricity to biological photosystems.

Here we design, assemble, and optimize a self-sustained hybrid photosynthesis system that aims to circumvent limitations in natural photosynthesis and artificial solar fuels approaches. The crux involves electrochemical reactivation of a PETC-modified cyanobacterium with no PSII activity and cannot perform photosynthesis alone. We introduce a strategy and device to shuttle high-energy electrons into this cyanobacterium under light illumination, demonstrating CO_2 conversion to fuel molecules such as acetate and amino acids[23-25]. Illuminating single photosystem (PSI) without the light absorption competition by the other (PSII) elevates efficiency ceiling of natural photosynthesis. The external electricity driving this reaction can be further harvested from multiple renewable sources, such as solar or wind, which are not limited by PAR and therefore enable a broader photosynthetic platform. This innovation introduces the concept of electro-synthetic cyanobacteria with the capability to drive carbon metabolism by both light energy and exogenous electricity. We describe this hybrid as an "electrophototrophic" system, a novel biotic-abiotic platform with the potential to valorize CO_2 in higher energy conversion efficiency than natural photosynthesis, while producing more complex hydrocarbon fuels than artificial photosynthesis.

A tailored photoelectrochemical system for electrophototrophy

To energize photosynthesis *via* extracellular electron transport, we first blocked the natural photosynthesis pathway in the cyanobacterium where initial electrons are generated from water splitting in PSII (Fig. 1a). This goal was achieved by either inhibiting PSII activity physiologically *via* site-specific inhibitors [26], or by leveraging a genetically generated PSII knockout mutant[27]. A mutant strain of the cyanobacterium *Synechocystis sp.* PCC 6803 (hereto *Synechocystis*), deficient in chlorophyll *a* binding protein (CP47) in PSII, cannot grow photoautotrophically. In the mutant (hereafter ΔPSII), PSII inactivity was shown by altered 77K fluorescence spectrum (Fig. S1b) and significantly decreased chlorophyll *a* level (Fig. S1c).

Next, we designed an electrochemical architecture (Fig. 1b) for exogenous electron delivery to cyanobacteria. This architecture allows physical attachment of cyanobacterial cells to carbon felt and the transparent cathodic fluorine-doped tin oxide

(FTO) electrode allows us to investigate light-activated photosystem driven by extracellular electricity. FTO glass substrate faced-up porous carbon felt offers extremely large interfacial area for bacteria loading (as shown in Fig. S2), excellent electron transport properties, as well as short active species diffusion length for efficient electrochemical reactions[28].

Light-dependent exogenous electron transfer to PETC

Electrochemical devices for electrogenesis from photoautotrophically grown *Synechocystis* on anode were reported previously[19,22,29]. We first reproduced this electrogenesis process in our newly designed system and examined its electrochemical properties by interfacing biocompatible porous carbon felt with wild type (WT) *Synechocystis* cells (Fig. 1b). WT *Synechocystis* cells displayed a strong electrogenic response to chopped light (Fig. 2a left axis, red solid line), suggesting that physical contact between cells and the extracellular electron-transduction surface enables interfacial electron transfer. In contrast, no photocurrent was observed when applying anode potential (0.4 V vs. Ag/AgCl) to ΔPSII (Fig. 2a left panel, red dash line), consistent with previous reports that PSII is the primary source for electrogenesis [21,29].

We next analyzed the properties of ΔPSII as an electron acceptor by applying cathodic potential (-0.7 V vs. Ag/AgCl). Intriguingly, illumination of ΔPSII under cathodic potential consistently increased cathodic current density (Fig. 2a left panel, black solid line), whereas the WT *Synechocystis* which carries functional PSII did not produce a photoelectrical response under cathodic bias (Fig. 2a left panel, black dash line). This result implies that active PETC components downstream of PSII in the ΔPSII mutant can accept electrons from the external circuit in lieu of the deactivated PSII. Without redox reactions by PSII, the light-dependent current response in ΔPSII is in line with the photo-reductive activity of PSI, the excitation of which can transfer electrons to the end of PETC, thus allowing continuous electron input from external circuit. In contrast, photoexcited PSII in the WT strain serves as the predominant electron donor, which could saturate the PETC and diminish photoelectrical response significantly when injecting exogenous electrons from cathode.

We next use site-specific redox inhibitors to demonstrate that PETC components downstream of PSII (see Fig. 1a) play a central role in electron flow from extracellular circuit to cyanobacteria. Supplementation of the herbicide (3-3,4-dichlorophenyl)-1,1-dimethylurea (DCMU), a specific inhibitor that blocks the binding site of Q_B in the photosystem[30] (Fig. S3) did not diminish the light-dependent electrical response in ΔPSII cells (Fig. 2b), suggesting that exogenous electrons can flow into the PETC downstream of Q_B. Either blocking cytochrome b6f activity with 2,5-dibromo-3-methyl-6-isopropylbenzoquinone (DBMIB)[31] or inhibiting ferredoxin and NADP reduction with phenylmercuric acetate (PMA)[32] resulted in a significant decrease in photoelectrical activity, as evinced by negligible changes of photocurrent density under light on and off (Fig. 2b). These site-specific inhibitions support the mechanism that exogenous electrons flow through cytochrome b6f, PSI and ultimately reach ferredoxin-NADP oxidoreductase in the PETC. The opposing effect of DBMIB and DCMU further implies that PQ is probably the entry point of exogenous electrons as it is the only PETC component between Q_B and cytochrome b6f.

Exogenous electrons energize CO_2-to-fuels conversion with high energy efficiency

Motivated by global demand in CO_2 recycling and energy production, we ask whether the exogenous electrons in our hybrid "electrophototrophic" system is able to energize CO_2 fixation and conversion to hydrocarbon fuels or fuel feedstocks. To answer this question, we incubated ΔPSII cultures and applied electrical potential with amperometric characterization. Light and electrical bias were systematically investigated as two key variables, and we observe photosynthetic CO_2 fixation and carbon product formation only when supplying both illumination and exogenous electron supply (Fig. S4-S6, more discussion in Supplementary Text). Shown in Fig. 3a, illumination on the cathode (typical white LED for plant growth, 55 μmol m^{-2} s^{-1} on FTO glass) led to a 3.5-fold increment of acetate production compared to its initial value with applied electrical bias (-0.7 V vs. Ag/AgCl, intermittent supply, Fig. S4). In the dark, acetate concentrations in the culture slightly decreased (from ~270 μM initial residual to ~100 μM), presumably due to non-photoexcited PSI which cannot reduce NADP and fuel carbon metabolism.

The viability determined by optical density (OD_{730}) measurements indicate slight increase under illumination, while the OD_{730} gradually declined ~40% in dark after 8 days (Fig. S5). In terms of exogenous electron supply, without negative electrical bias, no acetate production was detected even though cells were illuminated constantly (Fig. S6).

As shown in Fig. 3b, acetate production by illuminated ΔPSII was not found within the first 5 days for application of either no bias or -0.5 V vs. Ag/AgCl. In comparison, once more negative bias (-0.7 V vs. Ag/AgCl, intermittent supply, Fig. S4) was applied (day 6-10), acetate production resumed. Fig. S7 displays acetate yield as a function of various potentials (-0.15 to -0.7V) and indicates that potentials more negative than -0.6 V vs. Ag/AgCl can drive acetate production. Consistently, this threshold potential of -0.6 V (vs. Ag/AgCl) is near the standard reducing potential of electrons in photoexcited PSII (Fig. S7). This correlation implies a thermodynamic overpotential which could favor exogenous electrons flowing into the bacteria downstream of PETC. Fig. 3b demonstrates that acetate concentration in medium increased steadily for 5 days during incubation under -0.7 V, eventually reaching 650μM. Cell counts for ΔPSII, inferred by OD_{730} measurements, decreased unless a certain bias was applied (Fig. S8). These results support our hypothesis that the primary metabolic processes such as metabolite production and cell maintenance can be energized by highly reductive exogenous electrons, flowing through the PETC.

To further investigate the metabolic activities that can be driven by this electrophototrophic system, we performed an isotope tracer analysis by adding ^{13}C-sodium bicarbonate into the ΔPSII culture on cathode. Bicarbonate can be converted to CO_2 by cyanobacterial carbonic anhydrase[33]. This CO_2 can then drive carbon product formation (acetate) and/or be fixed into biomass *via* cell metabolism. We first examined the labeling fraction of acetate excreted into the medium. The GC-MS revealed the production of ^{13}C-acetic acid, indicating that newly fixed carbons end into this C2 product (Fig. 3c). ^{1}H-NMR spectra demonstrate that acetate was labeled in both methyl and carboxyl carbons (Fig. S9) and allow us to evaluate the energy conversion efficiency in the electro-photosynthetic process. Similar to the faradaic efficiency of conventional electrochemical processes, the exogenous electrons involved in electrophototrophic synthesis of acetate can be quantified by defining the exogenous electrons uptake

efficiency ($EEUE_{acetate}$). Over half (61.8%) of exogenous electrons were utilized by ΔPSII for selective acetic acid generation. Taking the incident photon flux into account, the overall energy conversion efficiency is approximately 9.32% (see Supplementary Text and Table S2). Even though this estimation only reflects the fixed carbons in acetate and does not those fixed into biomass (*vide infra*), the value still exceeds typical natural energy conversion efficiency of higher plants (<1%) and cyanobacteria (~4-7%).[34,35]

We next analyzed the labeling patterns of seven proteinogenic amino acids that are digested from cell biomass and are directly produced from the central carbon metabolism (Fig. 3d). After four days incubation of ΔPSII with ^{13}C-bicarbonate under constant white-light illumination, the cathodically biased cultures demonstrate partial ^{13}C-labeling in proteinogenic amino acids and display significantly higher fractional labeling (FL, denoting the proportion of labeled carbons) than the negative control cultures without applied bias. Serine, which can be synthesized from 3-phosphoglycerate, the first CO_2-fixation product of the CBB cycle, demonstrated a 3% FL in comparison with 1% in the negative control. This moderate ^{13}C-accumulation is real because we indeed detected significant increase of the m+1 ^{13}C-pattern in the carboxylic group of serine, consistent with the reaction skeleton of Ribulose-1,5-bisphosphate carboxylase/oxygenase (RuBisCO) (Table S1). As another major CO_2 entry point, ^{13}C-bicarbonate can be fixed by amphibolic reactions (*e.g.* phosphoenolpyruvate carboxylase) to generate oxaloacetate which is the precursor of aspartate and threonine. Consistently, biased cultures have much higher FL (7%) in these two amino acids than those in the unbiased cultures (1%).

Interestingly, we observed a new CO_2 fixation pathway activated in cyanobacteria *via* glycine cleavage system which was found in *Synechocystis*[36] but with no detailed *in vivo* characterization. The metabolic activity of this CO_2-fixing pathway can be reflected by the extremely high fractional labeling in glycine over 30% when incubated ΔPSII with ^{13}C-bicarbonate under constant white-light illumination for four days. Through this pathway, CO_2 will enter the one-carbon (C1) metabolism *via* formate which then forms the methylene group of glycine. The GC-MS fragment of glycine (Gly_85) represents this methylene group, demonstrating high FL (30%) consistently. Our ^{13}C-tracer analysis as well as extracellular metabolite analysis support that exogenous electron supply to

214 cyanobacterial PETC may lead to CO_2 fixation and conversion, demonstrating a
215 functional bioenergetics system that fuels endergonic metabolism.

216

217 **Discussion**

218 This work provides electrochemical and biochemical evidence to support a proof-
219 of-concept hybrid electro-photosynthetic system that leverages exogenous electrons to
220 supplement photosynthetic energy conversion for driving CO_2 fixation and conversion.
221 Cyanobacterial cells without PSII can sustain their metabolic viability on an electrode
222 surface and produce acetate, the primary excreting product (Fig. 3). Growing
223 photosystems-modified cyanobacteria in a photo-electrochemical architecture allows us
224 to expand the means by which photosynthetic organisms produce fuels and chemicals.
225 Such hybrid systems can access new pathways beyond canonical photosynthesis, the
226 inefficiency of which largely arises from the use of two photochemical systems with similar
227 absorption thresholds. The two photosystems (PSII, PSI) compete for the same regions
228 of the solar spectrum, cutting the energy efficiency nearly in half compared with what
229 might be achieved if the bandgaps were optimized to use different regions of the
230 spectrum[35,37]. From a broad standpoint, this work validates the first step of a new
231 photosynthesis concept to elevate the photosynthesis efficiency ceiling: Powering single
232 light-absorbing photosystem (PSI) *via* exogenous electricity which can be generated by
233 PV with extended range of solar energy absorption. Increases in efficiencies might be
234 obtained by PV devices that use the blue and near-UV region of the solar spectrum more
235 effectively or capture the energy of the sub-bandgap IR photons (illustrated in Fig. 4)[35].
236 Such strategies may be promising for increasing the theoretical upper bound of natural
237 photosynthesis, as proposed by Blankenship and co-authors[35].

238 Another merit for this hybrid photosynthesis approach arises from the fact that
239 inactivated PSII does not evolve O_2 as the photosynthetic byproduct. Suppressed O_2
240 evolution minimizes the propensity for RuBisCO to fix O_2 as a competitive substrate for
241 CO_2. In natural photosynthesis, substrate competition initiates an energy-intensive
242 recovery process of photorespiration[38] that can consume up to 25% of the initially stored
243 energy[39], a substantial source of inefficiency. Interestingly, although photorespiration also

plays a biosynthetic role in metabolic processes, *e.g*. supplying glycine as an essential metabolite[38], this role in hybrid photosynthesis seems to be substitutable with redundant pathways, such as glycine cleavage system[36]. This notion is strongly supported by the presence of pathway genes in cyanobacterial genome in line with isotope labeling patterns as we provided here. Decrease in photorespiration thus underlie new opportunities in the hybrid system to raise theoretical limits of photosynthesis.

More importantly, the hybrid system introduces a unique strategy for managing photosynthetic outcomes. In natural photosynthesis, linear electron flow occurring between two photochemical systems produces ATP and NADPH as energetic currency, and their proportions are regulated for various biosynthetic purposes. Phototrophs containing only PSI implement electron transport whereby electrons can be recycled from either reduced ferredoxin or NADPH to PQ, and subsequently to the cytochrome b6f complex[40]. Such *cyclic flow* generates a pH gradient (and thus ATP), but without the accumulation of reduced species for biosynthesis [41]. However, this study shows that *Synechocystis* carrying single PSI can be electrically energized to fix CO_2 and generate building blocks of biomass, evinced by labeled proteinogenic amino acids from ^{13}C-bicarbonate. This study further indicates that the hybrid photo-electrochemical process demonstrated here could enable on-demand control over the proportion of linear versus cyclic electron flow to tailor the stoihiometric ratios of ATP and NADPH and ultimate photosynthetic products. To achieve this goal, Nature evolved complicated regulatory mechanisms to tune the ratio of PSI to PSII[42,43]. In the photo-electrochemical hybrid demonstrated here, the ratios of energetic currency and products could instead be regulated through the injection of exogenous electrons, which creates an artificial linear electron flux that can be varied on-demand relative to cyclic electron flow by tuning the cathodic current density and/or incident photon flux. Since this hybrid approach is not tailored by evolution, it will be less constrained by the natural needs/environments to implement. Instead, the hybrid can be optimized in well-designed conditions for targeted ATP/NADPH ratio. Reengineering the system, for example on the biotic-abiotic interface, is expected to improve overall efficiency for tunable electron transfer.

Taken together, the hybrid electrophototroph as we demonstrate, drives exogenous electrochemical energy to replenish the universal energy and redox currency

in living cyanobacteria for biosynthesis. Considering its functionality and a number of advantages over pure natural/artificial photosynthesis, we posit that the development of this bio-electrochemical platform will pave a new avenue to couple renewable electricity with photobiological activities, a practical approach for production of hydrocarbon fuels from sun and CO_2.

Methods

Characterization of PSII knockout mutant in *Synechocystis*

The PSII deficient *Synechocystis* was a gift from Dr. Wim Vermaas at Arizona State University. This mutant was generated by deleting the psbB gene which encodes chlorophyll-binding protein CP-47 in PSII of *Synechocystis*.[27] The *slr0906* open reading frame (ORF) encoding psbB was disrupted by inserting an antibiotic-resistance gene cassette, replacing a part of the coding sequence. The genotype of the mutant was verified by a PCR analysis using primers 0906_VF and 0906_VR (0906-VF: CGTTACTAGAAGGAGCGTCA, 0906-VR: GGTACCTGGGGAGAGTAGAT). The ΔPSII mutant and wild type *Synechocystis* were measured by fluorescence emission spectra (77K) using a 435-nm excitation wavelength. The chlorophyll *a* level in the mutant was quantitated after methanol extraction by measuring the absorbance of the supernatant at 663 nm, using glass cuvettes.

Cyanobacteria-electrode hybrid system

The PSII deficient *Synechocystis* (Δslr0906) was first inoculated and cultured photoheterotrophically in BG11 medium with addition of 5mM glucose, under 30-50 $\mu E/m^2/s$ illumination at 30°C. Exponentially growing cells were collected for further applications.

In the following procedure, the tailored electrochemical H-cell with three-electrode configuration was applied for the electrochemical process. The reference and counter electrodes were silver/silver chloride electrode and Pt, respectively. The working electrode and reference electrode (CH Instruments, Inc.) were in the bottom chamber and the Pt wire counter electrode was in the top chamber. A Nafion 117 membrane (Sigma-

Aldrich) separates the two chambers. Each chamber has an inlet/outlet. The exponentially growing culture was centrifuged, separated from the supernatant and re-dispersed in the medium (BG11+ bicarbonate, pH = 7.8). A ~7 ml culture was transferred to the cathode chamber of the H-cell, where the culture was illuminated from the bottom transparent window. The device was air-tight and maintained at 30 °C for the duration of the electrochemical characterization.

Photoelectrochemical characterization

During the electrochemical incubation, a typical amperometry (i-t) procedure (CH Instruments, Inc.) was conducted to check the ability of ΔPSII cyanobacteria as an electron acceptor under illumination. It was conducted at different potentials (*vs.* Ag/AgCl). A 0.15 ml culture was taken every day for OD_{730} and metabolite analysis.

PETC inhibition assay

Three PETC inhibitors: 3-(3,4-dichlorophenyl)-1,1-dimethylurea (DCMU), 2,5-dibromomethylisopropyl-1,4-benzoquinone (DBMIB), and phenylmercury acetate (PMA) were obtained from Sigma-Aldrich. They were dissolved in dimethyl sulfoxide for use. The working concentrations of DCMU, DBMIB and PMA were based on previous report[21], which were 2 μM, 50 μM, 200 μM, respectively. The photoelectrochemical measurements were conducted after the inhibitors were supplemented into the culture for 10 min.

Electron microscopy characterization

After the electrochemistry process, the carbon felt electrode was fixed in 2.5% glutaraldehyde in phosphate buffer under 4 °C for 2 h. The samples then underwent a MilliQ water postfix wash and dehydration (~ 24 h in a high vacuum desiccator). Scanning Electron Microscopy (Hitachi S-4800 SEM) was applied to characterize the surface morphology. Samples were imaged at 3 kV acceleration, 7–10 mm working distance.

Quantitative analysis of acetate

We measured the excretion of acetate from *Synechocystis* using the following method. The culture samples were collected and the supernatant was separated from cells by filtration through 0.2 μM-diameter nylon membrane (Acrodisc®). Acetate concentration in each culture was analyzed with High Performance Liquid

Chromatography (HPLC, Agilent Technologies1200 series) by injecting 25 μL samples into an HPLC column (Bio-Rad Aminex HPX-87H), eluting with 5mM sulfuric acid at a flow rate of 0.6 ml/min, and detecting by a refractive index detector (retention time for acetate: 15.2 min). Standard samples with five different acetate concentrations (2.5, 5, 10, 25, and 50 mM) were used for quantification (R^2 = 0.99839).

^{13}C- isotope tracer analysis to track carbon fixation

^{13}C-bicarbonate was supplied during the electrochemical procedures to monitor carbon metabolism in the photoelectrochemical environment. The ^{13}C-labeled fraction of acetate and protein-bound amino acids were measured by NMR and gas chromatography-mass spectrometry (GC-MS), respectively. Exponentially growing ΔPSII cells were suspended in BG-11 medium supplemented with 100mM ^{13}C-labeled sodium bicarbonate. The culture was applied in the electrochemical device under sunlight simulated illumination (white LED, 55 μmol m^{-2} s^{-1}on FTO glass). Cultures were sampled at 0 hour, 2 day, 4 day and 5 day.

The sample treatment and GC-MS analysis were performed as previous reported.[44] Briefly, 5mL of sampled cultures were centrifuged at 10,000 g for 1 minute, the cell pellets were digested in 500μL 6M HCl at 105°C for 12 hours. The hydrolysate was dried under nitrogen gas flow at 65°C, dissolved in 50 μL water-free dimethylformamide. For the GC-MS measurement the proteinogenic amino acids were derivatized prior to analysis. The dried hydrolysate, dissolved in pyridine was derivatized by N-tert-butyldimethylsilyl-N-methyltrifluoroacetamide (TBDMS) with 1% tert-butyl-dimethylchlorosilane at 85°C for 60 min. 1 μL of the sample in the organic phase was loaded on the Agilent GC-6890 gas chromatography equipped with a Agilent 19091J-413 column (30m×0.32mm×0.25μm) directly connected to a MS-5975C mass spectrometer. Helium was used as the carrier gas. The oven temperature was initially held at 50°C for 2 min; then raised to 150°C at 5°C /min and held at that value for 2 min; finally, it was raised to 320°C at 7°C /min, and held at that final value for 2 min. Other settings included splitless and electron impact ionization (EI) at 70 eV. The FLs of alanine, aspartate, glutamate, glycine, phenylalanine, serine, threonine was analyzed.

To analyze the isotope labeling pattern of amino acids, a mass isotopomer distribution vector, MDV_{α}, was assigned according to Nanchen *et al* [45].

$$MDV_{\alpha} = \begin{bmatrix} (m_0) \\ (m_1) \\ \vdots \\ (m_n) \end{bmatrix} \quad \sum_{i=0}^{n} m_i = 1 \qquad (1)$$

where m_0 is the fractional abundance of molecules with mono-isotopic mass and $m_{i>0}$ is the abundance of fragments with heavier masses. The GC-MS data were corrected for the naturally occurring isotopes of oxygen (O), hydrogen (H) and carbon (C) atoms using a correction matrix (Eq. 2) as described by Nanchen *et al* [45].

$$MDV_{\alpha}^{*} = C_{corr,COH}^{-1} . MDV_{\alpha} \qquad (2)$$

where MDV_{α}^{*} is the corrected mass isotopomer distribution vector and $C_{corr,COH}^{-1}$ is the correction matrix. According to Equation 3, the resulting MDV_{α}^{*} values were then used to assess the fractional labeling (FL) of amino acids whose carbon skeletons are derived from their precursors in the central carbon metabolism.

$$FL = \frac{\sum_{i=0}^{n} i.mi}{n.\sum_{i=0}^{n} mi} \qquad (3)$$

where n represents the number of carbon atoms in the amino acid and i is the mass isotopomer. Corrected MDV for seven proteinogenic amino acids is shown in Table S1.

NMR samples were prepared by spiking neat solution with 50 microliters of D_2O with a 10x concentrated solution of Phosphate buffer and TMSP (Sodium-3-Trimethylsilylpropinoate-d4, Cambridge Isotopes), for a final solution of 550 microliters, 70 mM Phosphate buffer and 0.91 mM TMSP as an internal chemical shift and concentration standard. All ^{1}H NMR experiments were collected on a 600 MHz Bruker Avance III NMR spectrometer equipped with a Bruker 5 mm 1H/X broadband probe with sample temperature controlled at 25°C. Acquisition parameters were as follows: the 1D NOESY-presaturation experiment was used (Bruker pulse program noesypr1d) with a water presaturation pulse equivalent to 12 Hz field strength during both a 5 second

relaxation delay and during a 50 millisecond NOESY mixing time. Data was collected with a 20 ppm spectral window, 256 scans with 8 dummy scans, and 128k acquired points equivalent to 5.5 seconds of acquisition time. All spectra were processed using MestreNova version 14, which included 0.2 Hz exponential line-broadening before Fourier transform, manual phase correction, polynomial baseline correction, and chemical shift referencing to TMSP at 0.0 ppm. To obtain quantifications and isotopomer ratios, ^{1}H spectral deconvolution was performed using the MestreNova Line Fitting tool. Peak areas were exported to Microsoft Excel for further analysis.

References

1 Nichols, E. M. *et al.* Hybrid bioinorganic approach to solar-to-chemical conversion. *Proc Natl Acad Sci U S A* **112**, 11461-11466 (2015).

2 Liu, C., Colón, B. C., Ziesack, M., Silver, P. A. & Nocera, D. G. Water splitting–biosynthetic system with CO_2 reduction efficiencies exceeding photosynthesis. *Science* **352**, 1210-1213 (2016).

3 Sahoo, P. C., Pant, D., Kumar, M., Puri, S. K. & Ramakumar, S. S. V. Material–Microbe Interfaces for Solar-Driven CO_2 Bioelectrosynthesis. *Trends in Biotechnology*(2020).

4 Hohmann-Marriott, M. F. & Blankenship, R. E. Evolution of Photosynthesis. *Annual Review of Plant Biology* **62**, 515-548 (2011).

5 Nugent, J. H. A. Oxygenic Photosynthesis. *European Journal of Biochemistry* **237**, 519-531 (1996).

6 Georgianna, D. R. & Mayfield, S. P. Exploiting diversity and synthetic biology for the production of algal biofuels. *Nature* **488**, 329 (2012).

7 Rosenbaum, M., He, Z. & Angenent, L. T. Light energy to bioelectricity: photosynthetic microbial fuel cells. *Current Opinion in Biotechnology* **21**, 259-264 (2010).

8 Nozzi, N. E., Oliver, J. W. K. & Atsumi, S. Cyanobacteria as a Platform for Biofuel Production. *Frontiers in bioengineering and biotechnology* **1**, 7-7 (2013).

9 Xiong, W. *et al.* The plasticity of cyanobacterial metabolism supports direct CO_2 conversion to ethylene. *Nature Plants* **1**, 15053 (2015).

10 Lan, E. I. & Liao, J. C. ATP drives direct photosynthetic production of 1-butanol in cyanobacteria. *Proceedings of the National Academy of Sciences* **109**, 6018-6023 (2012).

11 Kusakabe, T. *et al.* Engineering a synthetic pathway in cyanobacteria for isopropanol production directly from carbon dioxide and light. *Metabolic Engineering* **20**, 101-108 (2013).

12 Schirmer, A., Rude, M. A., Li, X., Popova, E. & del Cardayre, S. B. Microbial Biosynthesis of Alkanes. *Science* **329**, 559-562 (2010).

13 Singh, A. K. & Mallick, N. Advances in cyanobacterial polyhydroxyalkanoates production. *FEMS Microbiology Letters* **364**(2017).

14 Pospíšil, P. Production of reactive oxygen species by photosystem II. *Biochimica et Biophysica Acta (BBA) - Bioenergetics* **1787**, 1151-1160 (2009).

15 Dogutan, D. K. & Nocera, D. G. Artificial Photosynthesis at Efficiencies Greatly Exceeding That of Natural Photosynthesis. *Accounts of Chemical Research* **52**, 3143-3148 (2019).

16 Nocera, D. G. The Artificial Leaf. *Accounts of Chemical Research* **45**, 767-776 (2012).

17 Lewis, N. S. Research opportunities to advance solar energy utilization. *Science* **351**, aad1920 (2016).

18 Cook, T. R. *et al.* Solar Energy Supply and Storage for the Legacy and Nonlegacy Worlds. *Chemical Reviews* **110**, 6474-6502 (2010).

19 Pisciotta, J. M., Zou, Y. & Baskakov, I. V. Light-dependent electrogenic activity of cyanobacteria. *PLoS One* **5**, e10821-e10821 (2010).

20 Tanaka, K., Kashiwagi, N. & Ogawa, T. Effects of light on the electrical output of bioelectrochemical fuel-cells containing Anabaena variabilis M-2: Mechanism of the post-illumination burst. *Journal of Chemical Technology & Biotechnology* **42**, 235-240 (1988).

21 Torimura, M., Miki, A., Wadano, A., Kano, K. & Ikeda, T. Electrochemical investigation of cyanobacteria Synechococcus sp. PCC7942-catalyzed photoreduction of exogenous quinones and photoelectrochemical oxidation of water. *Journal of Electroanalytical Chemistry* **496**, 21-28 (2001).

22 Sawa, M. *et al.* Electricity generation from digitally printed cyanobacteria. *Nat Commun* **8**, 1327-1327 (2017).

23 Levy, P. F., Sanderson, J. E., Kispert, R. G. & Wise, D. L. Biorefining of biomass to liquid fuels and organic chemicals. *Enzyme and Microbial Technology* **3**, 207-215 (1981).

24 Steinbusch, K. J. J., Hamelers, H. V. M., Plugge, C. M. & Buisman, C. J. N. Biological formation of caproate and caprylate from acetate: fuel and chemical production from low grade biomass. *Energy Environ. Sci.* **4**, 216-224 (2011).

25 Holtzapple, M. T. *et al.* in *Twentieth Symposium on Biotechnology for Fuels and Chemicals* (eds Davison B.H. & Finkelstein M.) Ch. Chapter 56, 609-631 (Humana Press, 1999).

26 Trebst, A. in *Methods in Enzymology* Vol. 69 (ed Anthony San Pietro) 675-715 (Academic Press, 1980).

27 Vermaas, W. F. J., Williams, J. G. K., Rutherford, A. W., Mathis, P. & Arntzen, C. J. Genetically engineered mutant of the cyanobacterium *Synechocystis* 6803 lacks the photosystem II chlorophyll-binding protein CP-47. *Proceedings of the National Academy of Sciences* **83**, 9474-9477 (1986).

28 Zhu, C., Li, H., Fu, S., Du, D. & Lin, Y. Highly efficient nonprecious metal catalysts towards oxygen reduction reaction based on three-dimensional porous carbon nanostructures. *Chem Soc Rev* **45**, 517-531 (2016).

29 Saar, K. L. *et al.* Enhancing power density of biophotovoltaics by decoupling storage and power delivery. *Nature Energy* **3**, 75-81 (2018).

30 Mackay, S. P. & O 'Malley, P. J. Molecular Modelling of the Interaction between DCMU and the Q_B-Binding Site of Photosystem II. *Zeitschrift für Naturforschung C* **48**, 191-198 (1993).

31 Roberts, A. G., Bowman, M. K. & Kramer, D. M. The inhibitor DBMIB provides insight into the functional architecture of the Qo site in the cytochrome *b6f* complex. *Biochemistry* **43**, 7707-7716 (2004).

32 Honeycutt, R. C. & Krogmann, D. W. Inhibition of chloroplast reactions with phenylmercuric acetate. *Plant Physiol* **49**, 376-380 (1972).

33 Aizawa, K. Carbonic anhydrase and CO_2 concentrating mechanisms in microalgae and cyanobacteria. *FEMS Microbiology Letters* **39**, 215-233 (1986).

34 Hambourger, M. *et al.* Biology and technology for photochemical fuel production. *Chem Soc Rev* **38**, 25-35 (2009).

35 Blankenship, R. E. *et al.* Comparing photosynthetic and photovoltaic efficiencies and recognizing the potential for improvement. *Science* **332**, 805-809 (2011).

36 Wittmiß, M., Mikkat, S., Hagemann, M. & Bauwe, H. Stoichiometry of two plant glycine decarboxylase complexes and comparison with a cyanobacterial glycine cleavage system. *The Plant Journal* **103**, 801-813 (2020).

37 Hanna, M. C. & Nozik, A. J. Solar conversion efficiency of photovoltaic and photoelectrolysis cells with carrier multiplication absorbers. *Journal of Applied Physics* **100**, 074510 (2006).

38 Foyer, C. H., Bloom, A. J., Queval, G. & Noctor, G. Photorespiratory Metabolism: Genes, Mutants, Energetics, and Redox Signaling. *Annual Review of Plant Biology* **60**, 455-484 (2009).

39 Zhu, X.-G., Long, S. P. & Ort, D. R. Improving Photosynthetic Efficiency for Greater Yield. *Annual Review of Plant Biology* **61**, 235-261 (2010).

40 Yamori, W. & Shikanai, T. Physiological Functions of Cyclic Electron Transport Around Photosystem I in Sustaining Photosynthesis and Plant Growth. *Annual Review of Plant Biology* **67**, 81-106 (2016).

41 Williams, J. G. K. in *Methods in Enzymology* Vol. 167 766-778 (Academic Press, 1988).

42 Murakami, A., Kim, S. J. & Fujita, Y. Changes in photosystem stoichiometry in response to environmental conditions for cell growth observed with the cyanophyte Synechocystis PCC 6714. *Plant Cell Physiol* **38**, 392-397 (1997).

43 Murakami, A. & Fujita, Y. Regulation of Stoichiometry between PSI and PSII in Response to Light Regime for Photosynthesis Observed with *Synechocystis* PCC 6714: Relationship between Redox State of Cyt b_6 *-f* Complex and Regulation of PSI Formation. *Plant Cell Physiol* **34**, 1175–1180 (1993).

44 Xiong, W., Liu, L., Wu, C., Yang, C. & Wu, Q. 13C-tracer and gas chromatography-mass spectrometry analyses reveal metabolic flux distribution in the oleaginous microalga Chlorella protothecoides. *Plant Physiol* **154**, 1001-1011 (2010).

45 Nanchen, A., Fuhrer, T. & Sauer, U. Determination of metabolic flux ratios from 13C-experiments and gas chromatography-mass spectrometry data: protocol and principles. *Methods Mol Biol* **358**, 177-197 (2007).

Acknowledgments

This work was authored in part by the National Renewable Energy Laboratory, operated by Alliance for Sustainable Energy, LLC, for the U.S. Department of Energy (DOE) under Contract No. DE-AC36-08GO28308. Funding provided by a Laboratory Directed Research and Development seed project at the National Renewable Energy Laboratory. The views expressed in the article do not necessarily represent the views of the DOE or the U.S. Government. The U.S. Government retains and the publisher, by accepting the article for publication, acknowledges that the U.S. Government retains a nonexclusive, paid-up, irrevocable, worldwide license to publish or reproduce the published form of this work, or allow others to do so, for U.S. Government purposes. We acknowledge Dr. Wim

Vermaas at Arizona State University for providing a Synechocystis PSII deficient mutant. We also thank Dr. Ji Hao for assistance on transport measurements.

Author contributions: W.X., J.B., D.S. project conception. Z.L., X.C., D.S., J.B., W.X. designed, performed, and/or analyzed photo-electrochemical experiments. Z.L., C.W., X.G., W.X. designed, performed, and/or analyzed biological experiments including cyanobacteria cultivation, spectroscopic analysis, metabolite analysis, ^{13}C-labeling and GC-MS. B.A. performed and analyzed NMR data. Z.L., W.X., J.B. wrote the manuscript with input from all authors and revisions from D.S. and J.Y.

Competing interests: Authors declare no competing interests**.**

Figures and figure legends

Figure 1

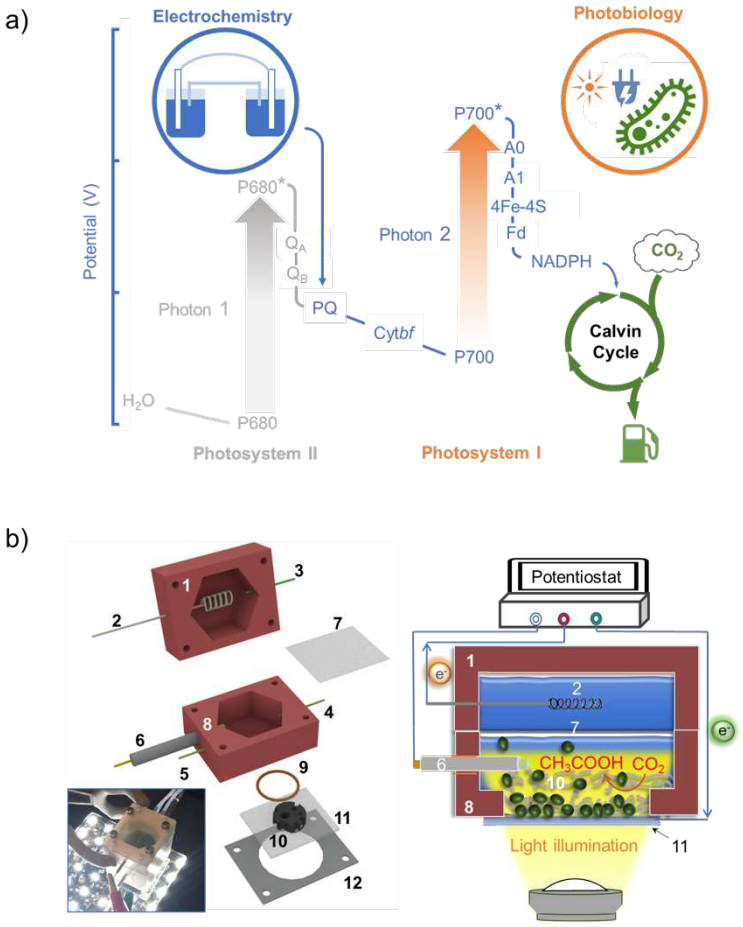

Fig. 1. Electrophototrophic system. **a)** The electrophototroph is designed for CO_2-to-fuels conversion with external supply of light and electricity to a tailored photosynthetic microbe. To this end, photosystem II in natural photosynthesis (gray) can be genetically removed, and instead the external electrochemical circuit delivers high-energy electrons to photoexcited photosystem I (oxidized P700), and ultimately produces NADPH to drive CO_2 fixation. This process could leverage electron acceptors in the PETC including plastoquinone (PQ), Cytochrome b6f complex (Cyt*bf*), special chlorophyl (A_0), vitamin K (A_1), iron-sulfur centers (4Fe-4S), and ferredoxin (fd) *etc*. Protons can be pumped across the thylakoid membrane establishing a proton-motive force that can be used for the synthesis of ATP. **b)** Schematic illustration and photograph (inset of left panel) of

electrochemical device to shuttle electrons to PSII deficient cyanobacteria. Component 1 and 8: PTFE anodic part and cathodic part; Component 2: Platinum counter electrode; Component 3, 4, 5: medium inlet/outlet; Component 6: Ag/AgCl reference electrode; Component 7: Nafion Membrane; Component 9: Seal O-ring; Component 10: Carbon felt; Component 11: FTO glass; Component 12: Working electrode clamp. Right panel shows the loading of cyanobacterial cells and the electrons delivery process.

Figure 2

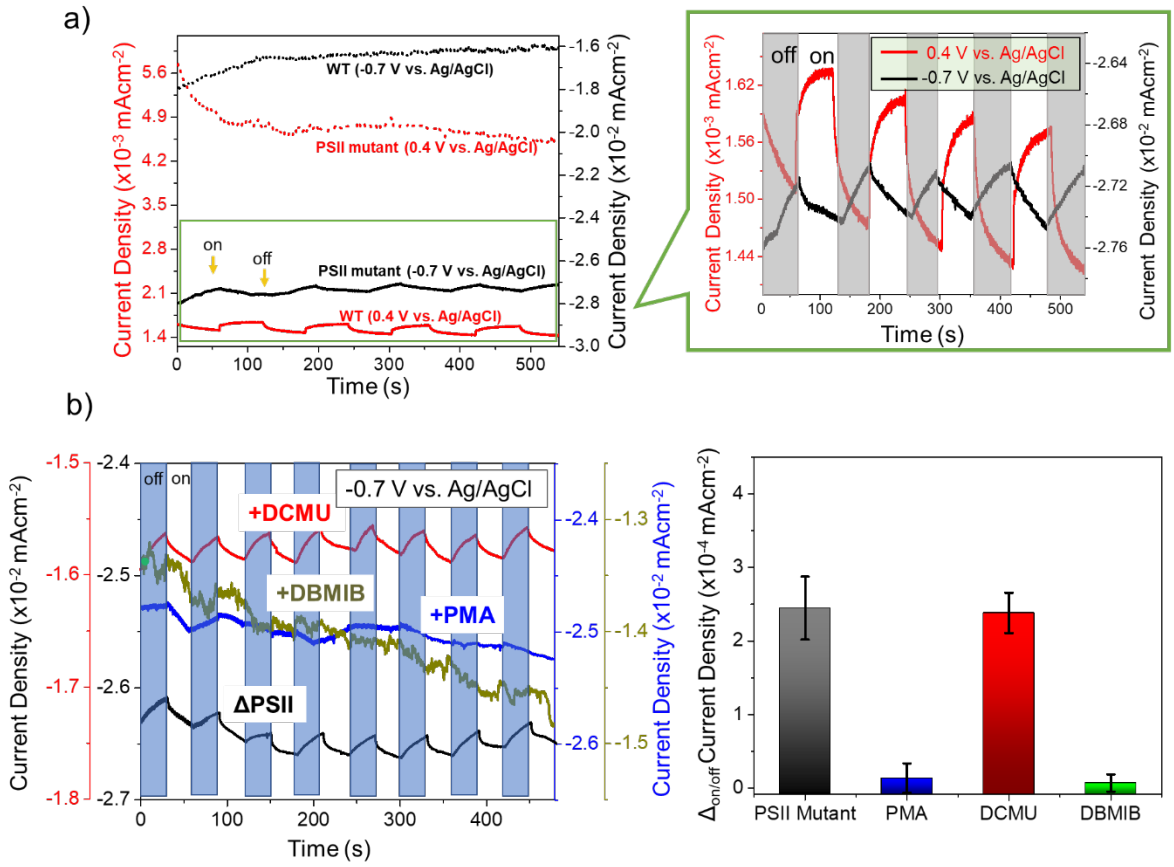

Fig. 2. Electrochemical properties of the electrophototrophic hybrid. **a)** i-t measurement under chopped illumination when cyanobacterial cells (*Synechocystis* WT and ΔPSII mutant) were applied as electron donor (on anode, red solid and dash line) or acceptor (on cathode, black solid and dash line). Right panel comparing the light-response of WT and ΔPSII cells as electron donor and acceptor, respectively. **b)** Current density changes in response to light/dark switch with addition of site-specific PETC inhibitors to cathodal ΔPSII culture. The time-course and differences of current density between light and dark are shown on the left and right panel, respectively.

Figure 3

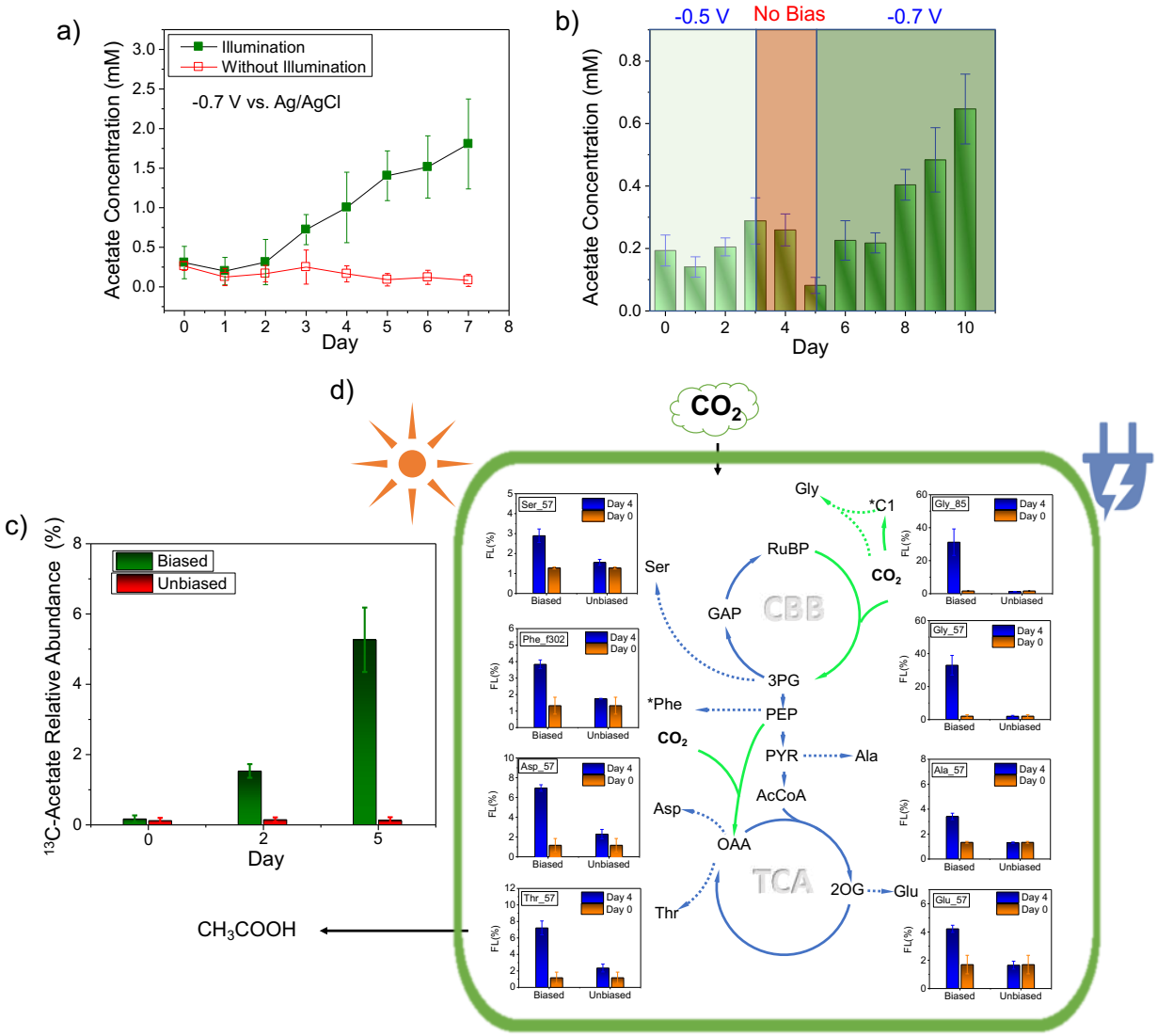

Fig. 3. CO_2 valorization by the electrophototrophic hybrid. **a)** Electrophototrophic acetate production of ΔPSII by external electrical bias (-0.7 V vs. Ag/AgCl) with and without illumination. **b)** Time course of electrophototrophic productivity for ΔPSII under illumination with different electron supplies. Error bars represent standard deviations from biological triplicates. **c)** ^{13}C-acetate production via fixation of $^{13}CO_2$ (derived from ^{13}C-bicarbonate) in illuminated ΔPSII, with or without application of external electrical bias (-0.7 V vs. Ag/AgCl). **d)** Fractional labeling of seven protein-bound amino acids that were directly produced from the central carbon metabolism via fixation of $^{13}CO_2$ (derived from ^{13}C-bicarbonate) in illuminated ΔPSII, with or without application of external electrical bias

(-0.7 V vs. Ag/AgCl). Green arrows indicate CO_2-fixing reactions. Dash lines are reactions for the synthesis of amino acids. Abbreviations: RuBP, ribulose 1,5-bisphosphate; GAP, glyceraldehyde 3-phosphate; 3PG, 3-phosphoglycerate; PEP, phosphoenolpyruvate; PYR, pyruvate; AcCoA, acetyl coenzyme A; OAA, oxaloacetate; 2OG, 2-oxoglutarate. CBB, the Calvin-Benson-Bassham Cycle; TCA, the tricarboxylic acid cycle. Amino acids are presented by their 3-letter abbreviations. *Phe indicates partial carbons of phenylalanine (C1-3) synthesized from PEP. *C1 indicates that one carbon unit is the precursor of glycine's methylene group and can be represented by the Gly_85 fragment in GC-MS.

Figure 4

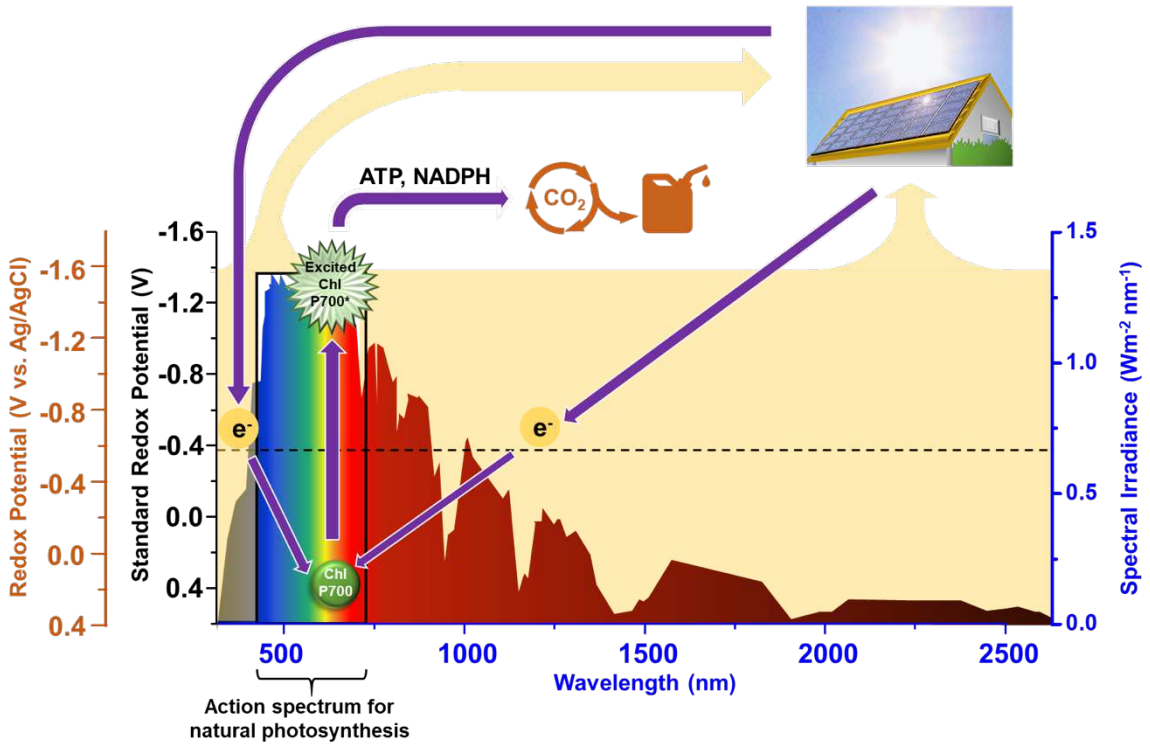

Fig. 4 Schematic illustration of a hybrid photosynthesis system to convert broader spectrum of PAR than natural photosynthesis. Leveraging PV device, UV-blue and IR regions that cannot be utilized by photosynthetic organisms, may be converted to electricity to energize electrophototrophic cyanobacteria with single PSI for CO_2 valorization. Dash line represents the standard redox potential where the exocellular electrons shuttled to the photosynthetic cells carrying a single photosystem.

Figures

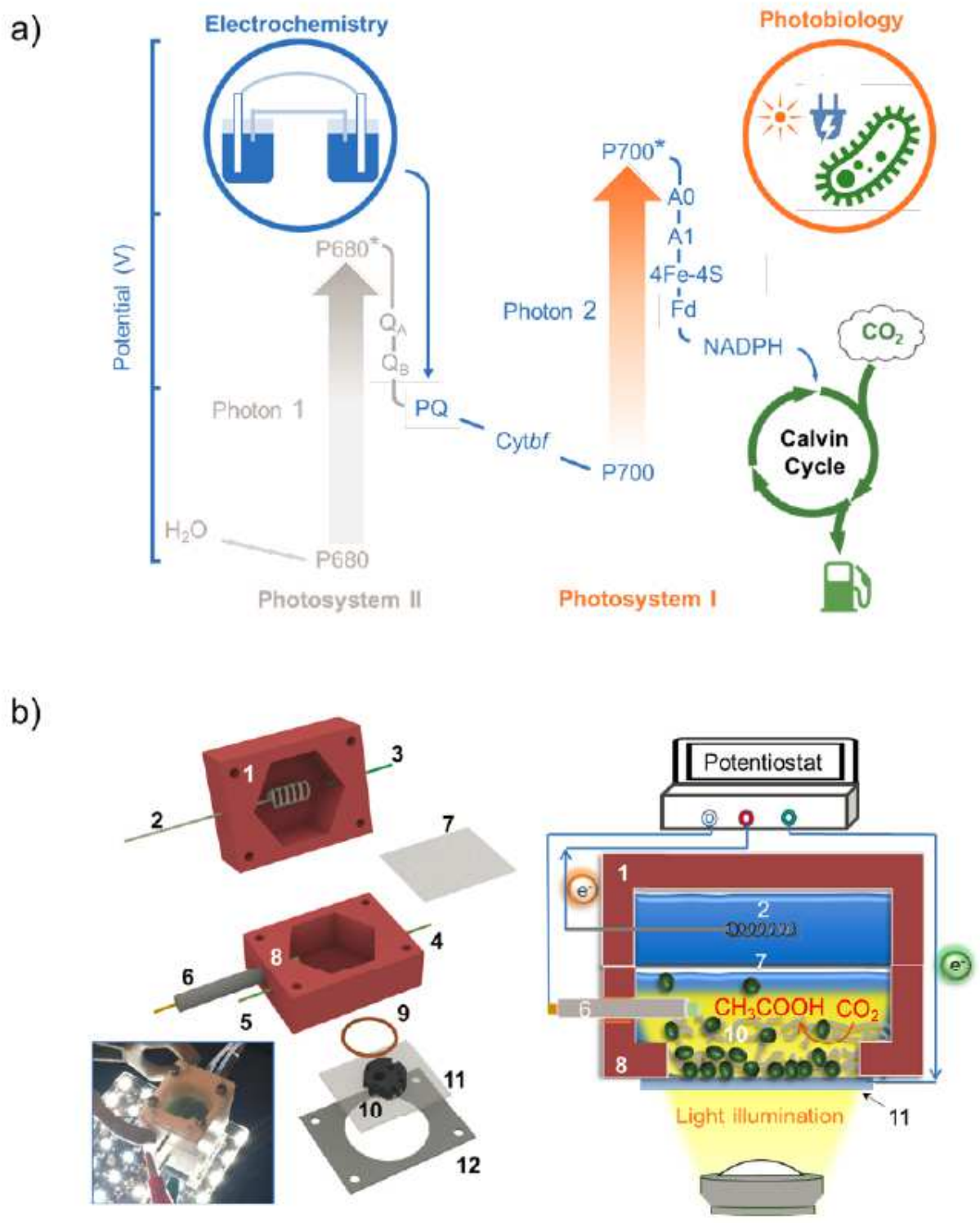

Figure 1

Electrophototrophic system. a) The electrophototroph is designed for CO2-to539 fuels conversion with external supply of light and electricity to a tailored photosynthetic microbe. To this end, photosystem II in natural photosynthesis (gray) can be genetically removed, and instead the external electrochemical circuit

delivers high-energy electrons to photoexcited photosystem I (oxidized P700), and ultimately produces NADPH to drive CO2 fixation. This process could leverage electron acceptors in the PETC including plastoquinone (PQ), Cytochrome b6f complex (Cytbf), special chlorophyl (A0), vitamin K (A1), iron-sulfur centers (4Fe-4S), and ferredoxin (fd) etc. Protons can be pumped across the thylakoid membrane establishing a proton-motive force that can be used for the synthesis of ATP. b) Schematic illustration and photograph (inset of left panel) of electrochemical device to shuttle electrons to PSII deficient cyanobacteria. Component 1 and 8: PTFE anodic part and cathodic part; Component 2: Platinum counter electrode; Component 3, 4, 5: medium inlet/outlet; Component 6: Ag/AgCl reference electrode; Component 7: Nafion Membrane; Component 9: Seal O-ring; Component 10: Carbon felt; Component 11: FTO glass; Component 12: Working electrode clamp. Right panel shows the loading of cyanobacterial cells and the electrons delivery process.

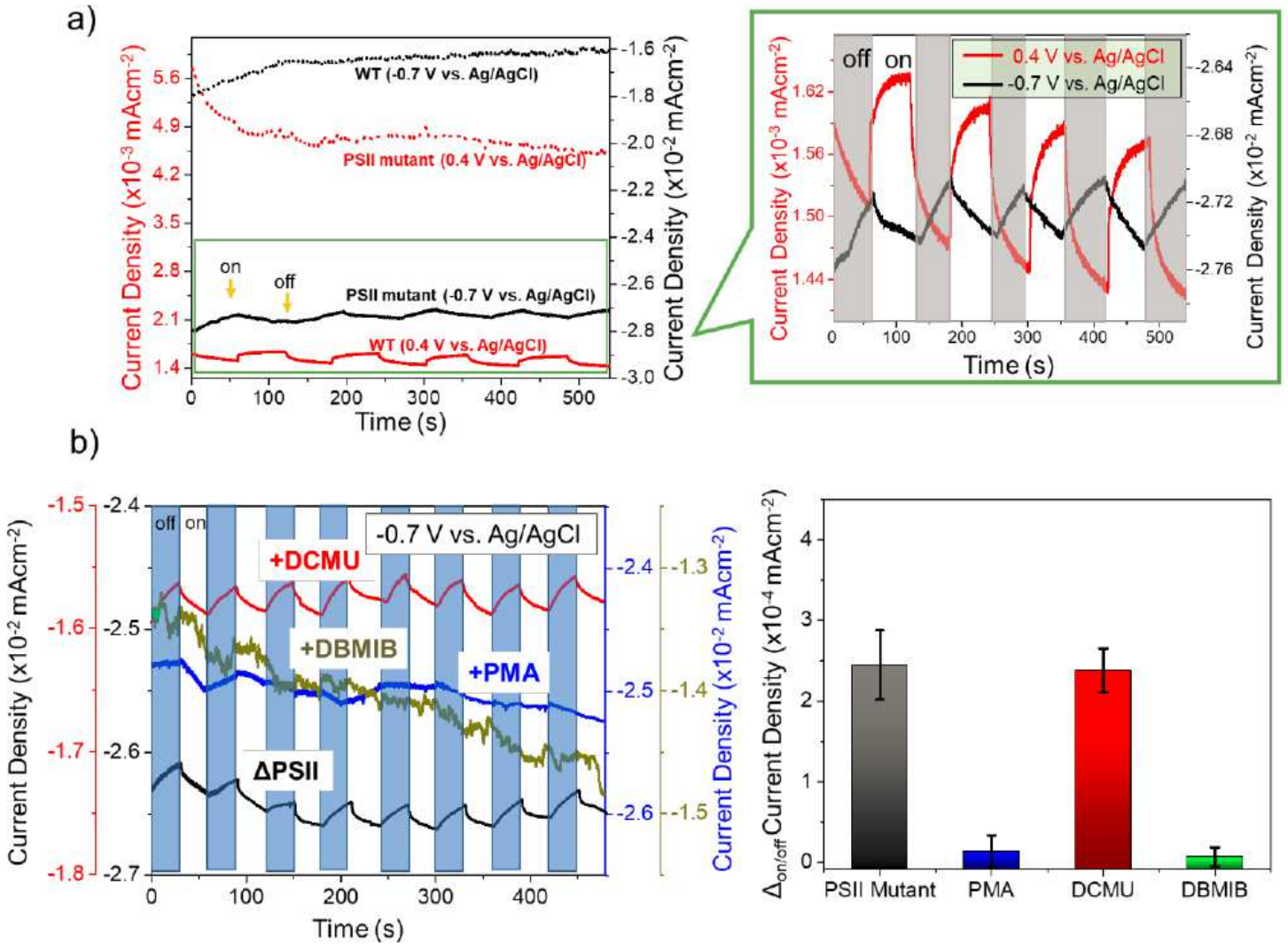

Figure 2

Electrochemical properties of the electrophototrophic hybrid. a) i-t measurement under chopped illumination when cyanobacterial cells (Synechocystis WT and ΔPSII mutant) were applied as electron donor (on anode, red solid and dash line) or acceptor (on cathode, black solid and dash line). Right panel

comparing the light response of WT and ΔPSII cells as electron donor and acceptor, respectively. b) Current density changes in response to light/dark switch with addition of site-specific PETC inhibitors to cathodal ΔPSII culture. The time-course and differences of current density between light and dark are shown on the left and right panel, respectively.

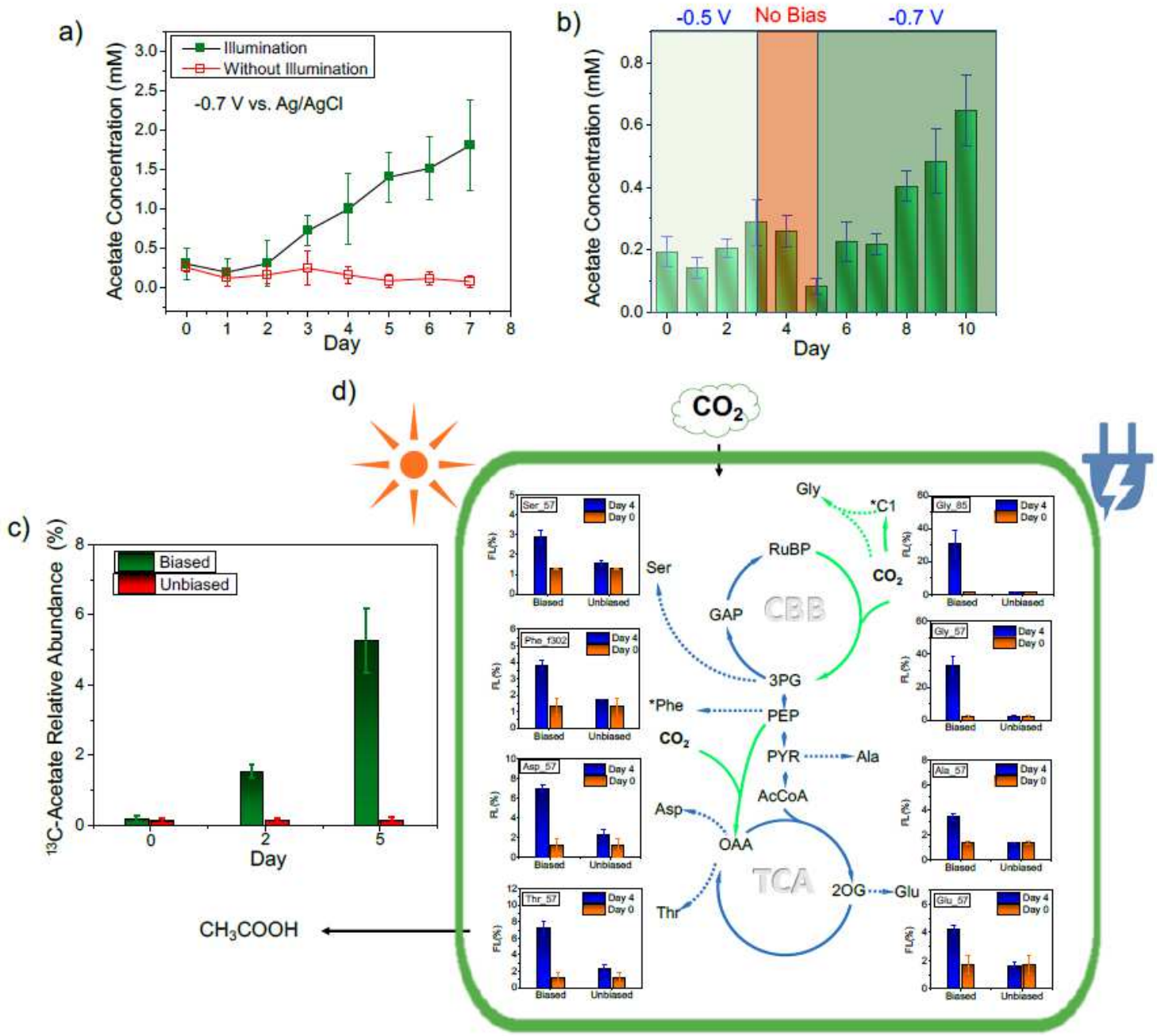

Figure 3

CO2 valorization by the electrophototrophic hybrid. a) Electrophototrophic acetate production of ΔPSII by external electrical bias (-0.7 V vs. Ag/AgCl) with and without illumination. b) Time course of electrophototrophic productivity for ΔPSII under illumination with different electron supplies. Error bars represent standard deviations from biological triplicates. c) 13C-acetate production via fixation of 13CO2 (derived from 13C bicarbonate) in illuminated ΔPSII, with or without application of external electrical bias

(- 0.7 V vs. Ag/AgCl). d) Fractional labeling of seven protein-bound amino acids that were directly produced from the central carbon metabolism via fixation of 13CO2 (derived from 13C-bicarbonate) in illuminated ΔPSII, with or without application of external electrical bias (-0.7 V vs. Ag/AgCl). Green arrows indicate CO2-fixing reactions. Dash lines are reactions for the synthesis of amino acids. Abbreviations: RuBP, ribulose 1,5-bisphosphate; GAP, glyceraldehyde 3-phosphate; 3PG, 3-phosphoglycerate; PEP, phosphoenolpyruvate; PYR, pyruvate; AcCoA, acetyl coenzyme A; OAA, oxaloacetate; 2OG, 2-oxoglutarate. CBB, the Calvin-Benson-Bassham Cycle; TCA, the tricarboxylic acid cycle. Amino acids are presented by their 3-letter abbreviations. *Phe indicates partial carbons of phenylalanine (C1-3) synthesized from PEP. *C1 indicates that one carbon unit is the precursor of glycine's methylene group and can be represented by the Gly_85 fragment in GC-MS.

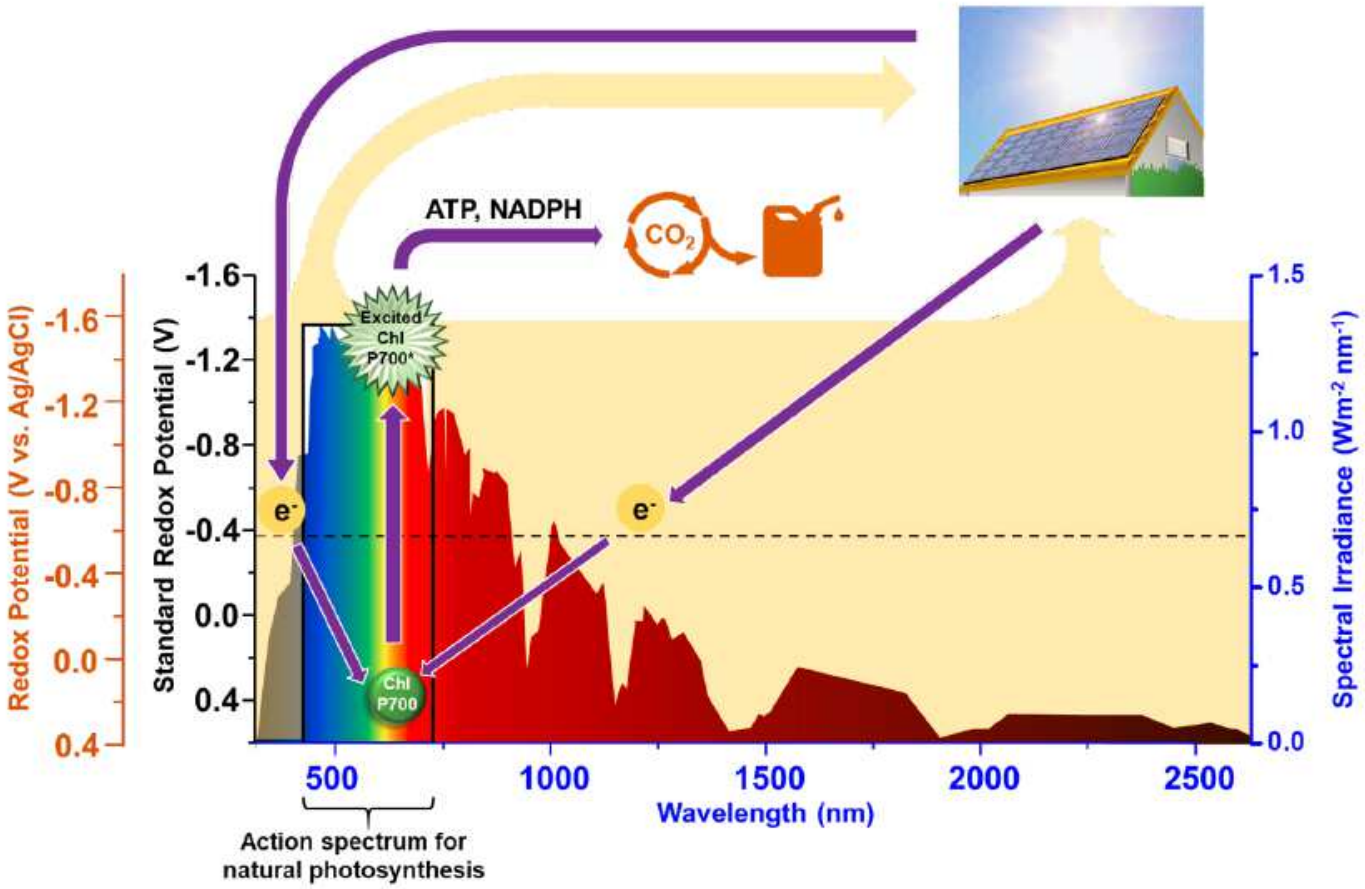

Figure 4

Schematic illustration of a hybrid photosynthesis system to convert broader spectrum of PAR than natural photosynthesis. Leveraging PV device, UV-blue and IR regions that cannot be utilized by photosynthetic organisms, may be converted to electricity to energize electrophototrophic cyanobacteria with single PSI for CO2 valorization. Dash line represents the standard redox potential where the exocellular electrons shuttled to the photosynthetic cells carrying a single photosystem.

Supplementary Files

This is a list of supplementary files associated with this preprint. Click to download.

- SupplementaryMaterials.pdf